Journal of Materials Chemistry

Cite this: J. Mater. Chem., 2012, 22, 9841

www.rsc.org/materials

PAPER

Ferroelastic phase transition and dielectric anomalies in 2,4,6-trimethylanilinium perchlorate†

Yi Zhang,[a] Kunio Awaga,[b] Hirofumi Yoshikawa[b] and Ren-Gen Xiong*[a]

Received 31st January 2012, Accepted 22nd March 2012
DOI: 10.1039/c2jm30581j

The crystal structure of the crystalline 1 : 1 complex of 2,4,6-trimethylaniline with perchloric acid, $(C_9H_{14}N)^+ \cdot ClO_4^-$ (**1**), was determined at 25 °C and 110 °C, respectively. The crystal structural analysis of both temperatures show that **1** undergoes a reversible phase transition from triclinic $P\bar{1}$ (No.2) to monoclinic $P2_1/m$ (No.11) with a distinct change of the cell parameters. It is a ferroelastic phase transition with an Aizu notation of $2/mF\bar{1}$. DSC (differential scanning calorimetry) measurement confirms that this compound undergoes a reversible first-order solid-state structural phase transition at about 48 °C with a thermal hysteresis of 3 °C. Usually, phase transition is accompanied by an anomaly of the dielectric constant near phase transition temperature (T_c). The DSC measurement, temperature-dependent single-crystal X-ray diffraction and dielectric studies reveal that **1** displays structural phase transitions and distinctly step-like dielectric anomalies at 48 °C probably supporting that this phase transition is of the first-order.

1. Introduction

For the last decade, special attention has been paid to ferroelastic materials due to their promising potential applications. Ferroelastics are potentially useful materials for nanotechnological applications as the ferroelastic twin patterns occur exactly on the nanometer scale and ferroelastic crystals may hold the key for templating electronic nanostructures.[1,2] The shape memory effect and superelasticity are also manifestations of ferroelasticity.[3–5] Nitinol (nickel titanium), a common ferroelastic alloy, can display either superelasticity or the shape-memory effect at room temperature, depending on the nickel/titanium ratio. Particularly, multiferroics, where (anti-) ferromagnetic, ferroelectric and ferroelastic order parameters coexist,[6–10] have become one of the most popular research topics, which enable manipulation of magnetic ordering and/or polarization ordering by an external stress through switching of the ferroelastic state.[1]

Ferroelasticity is a phenomenon in which a material may exhibit a spontaneous strain while the strain can be reversed by stress. When stresses are applied to objects, a linear elastic response is often observed for a large number of crystal, glass and many cross-linked polymers, which is called Hooke's law. Hooke's law is not valid in cellular structures like wood and in elastomers like rubber. Whatever, the recoverable strain in materials of either the linear or the nonlinear type is usually a single-value function of the small applied stress.[11] However, the strain in the ferroelastic crystals is a double-value function of applied stress and show hysteresis loops, which are similar to ferroelectric hysteresis loops. Such hysteresis is the basic character of the ferroelastic effect which is defined as the mechanical switching between either different crystal structures (*e.g.* cubic to tetragonal) or different orientations (a 'twin' phase). Although the atomic displacement mechanism captures the essential reason why a hysteresis can be observed, the actual switching mechanism is still elusive. For example, the energy stored in one hysteresis loop is much smaller than the energy required to switch all atoms from one configuration to another, which indicates that not all atoms take part in the switching process simultaneously.[12] The local ferroelastic switching may produce a high-energy domain state, leading to a relaxation of the smaller (switched) domain back to the original ferroelastic state.[13,14] Domain structure is an important ingredient in functionality of ferroelastic materials. It has impact on their nonlinear optical properties, dielectric permittivity, and polarization switching phenomena. Since domain boundaries in ferroelastic materials can simultaneously play the role of the ferroelastic walls, such domain walls also strongly influence the electromechanical material properties: they facilitate switching of spontaneous polarization and spontaneous deformation. The domain structure also provides additional degrees of freedom for tuning the material properties. Further development of domain engineering strategies requires deeper understanding of the physics of the ferroelastic domain wall itself.[1]

[a]*Ordered Matter Science Research Center, Southeast University, Nanjing 211189, P. R. China. E-mail: xiongrg@seu.edu.cn; Fax: (+86)-25-52090626*
[b]*Research Center for Materials Science and Department of Chemistry, Nagoya University, Furo-cho, Chikusa-ku, Nagoya 464-8602, Japan*

† Electronic supplementary information (ESI) available: IR, PXRD, crystal data and hydrogen-bond geometry of compound **1**. CCDC reference numbers 865148–865149. For ESI and crystallographic data in CIF or other electronic format see DOI: 10.1039/c2jm30581j

The ferroelastic properties are sensitive to thermodynamic parameters such as temperature T, pressure P or chemical composition N. Most ferroelastic materials show phase transitions from a paraelastic phase to a ferroelastic phase with decreasing temperature. However, the control of such ferroelastic switching in a single-phase system has been a significant challenge as elastic interactions tend to destabilize small switched volumes.[13,14] As it is rather a difficult experimental task to measure ferroelastic hysteresis with any acceptable degree of accuracy, it has become customary to call a material 'ferroelastic' if a phase transition occurs (or may be thought to occur) which may conceivably generate ferroelasticity.[12]

2. Experimental

2.1 Synthesis

The compound **1** was prepared by the dropwise addition of concentrated perchloric acid to a solution of 2,4,6-trimethylanline (1.35 g, 0.01 mol) in absolute ethanol (10 ml). The resulting white precipitate was filtered. High quality single crystals were obtained by evaporation from aqueous solution at room temperature. In the IR spectra (see Supporting Information, Fig. 1S†), several peaks at approximately 1580 cm^{-1} and 1600 cm^{-1} indicate the presence of benzene ring, while the peak at 3450 cm^{-1} may be attributed to the $-NH_3^+$ and the peak at 1375 cm^{-1} may be attributed to the $-CH_3$. The anions show strong infrared bands at 1100 cm^{-1} (ClO_4^-). The phase purity of **1** at room temperature was verified by powder XRD (PXRD) pattern (Fig. 2S†).

2.2 Single-crystal X-ray crystallography

X-Ray diffraction experiments were carried out on the compound using a Rigaku Saturn 924 diffractometer with Mo-Kα radiation (λ = 0.71073 Å) at various temperatures. Data processing including empirical absorption correction was performed using the Crystalclear software package (Rigaku, 2005). The structures were solved using direct methods and successive Fourier difference synthesis (SHELXS-97), and refined using the full-matrix least-squares method on F^2 using the SHELXLTL software package (Sheldrick, 2008). Non-H atoms were refined anisotropically using all reflections with $I > 2\sigma(I)$. All H atoms were placed in calculated positions and refined using "riding" model for aromatic ring H atoms with $U_{iso} = 1.2\ U_{eq}$ (C), methyl H atoms with $U_{iso} = 1.5\ U_{eq}$ (C) and ammonium H atoms with $U_{iso} = 1.5\ U_{eq}$ (N). The asymmetric units and the packing views were drawn with DIAMOND (Brandenburg and Putz, 2005) Visual Crystal Structure Information System Software. Crystallographic data and details of the data collection and refinement for 25 °C and 110 °C are summarized in Table 1 (Table 1S†).

2.3 Dielectric measurement

For the complex dielectric measurement the sample was made with the powder sample-pressed pellet of the compound **1**. The pressed-powder pellet deposited with carbon conducting glue was used for dielectric studies. Complex dielectric permittivity ε ($\varepsilon = \varepsilon' - i\varepsilon''$) was performed on pure compound **1** powder using automatic impedance TongHui 2828 Analyzer in the frequency range 10–1000 kHz. The measuring AC voltage was 1 V.

2.4 DSC measurement

DSC measurements were performed by heating and cooling the samples (20.8 mg) in the temperature range of 30–110 °C on PerkinElmer Diamond DSC instrument. The measurements were carried out under nitrogen at atmospheric pressure in aluminum crucibles with a heating rate of 5 °C min^{-1}.

2.5 Specific heat measurement

The measurement procedures can be referred to in the paper on powdered samples or polycrystals.[10]

3. Results and discussion

3.1 Thermal analysis

DSC measurement is usually used to detect whether the compound displays a reversible phase transition triggered by temperature or not. The DSC measurement for **1** is performed in the temperature region of 30–110 °C. The heating and cooling curves of **1** show one pair of reversible peaks, an exothermic peak at 44.7 °C and an endothermic peak at 47.7 °C (Fig. 1a). These observed peaks represent a reversible phase transition with a thermal hysteresis of 3 °C. The sharp peaks reveal the discontinuous character of the phase transition, being indicative of a first-order phase transition. Thus, for warming process, ΔH = 13.52 J g^{-1}; for cooling process, ΔH = 12.05 J g^{-1}, the averaged ΔH is estimated to be 12.79 J g^{-1}. For warming process, T_C = 320.7 K, ΔS = (12.79/320.7) J g^{-1} K^{-1} = 3.988 × 10^{-2} J g^{-1} K^{-1} while for the cooling process, T_C = 317.7 K, ΔS = (12.79/317.7) J g^{-1} K^{-1} = 4.026 × 10^{-2} J g^{-1} K^{-1}.

It is well-known that the shape of the specific heat plot will further confirm whether there is a phase transition occurring and the phase transition character. Fig. 1b shows that a peak appears at *ca.* 48 °C, surely manifesting the presence of a phase transition as a typical second-order one (non-λ-shape), like that of triglycine sulfate (TGS). However, it is very strange that the temperature-dependence of C_p goes down not like normal going up. This phenomenon will be under study (experimental results repeated 2–3 times, reproducible).

3.2 Crystal structure

The phase transition was confirmed by the determination of variable-temperature crystal structures of the compound **1**. In

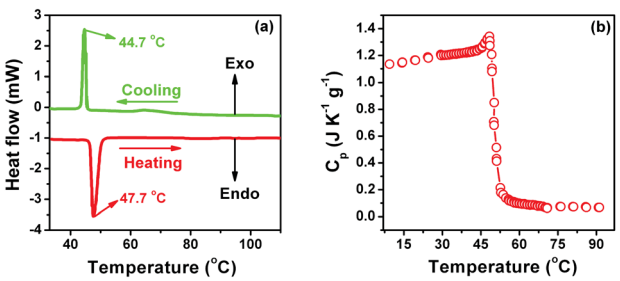

Fig. 1 (a) DSC measurement result of **1**. (b) Specific heat (C_p) diagram of **1**.

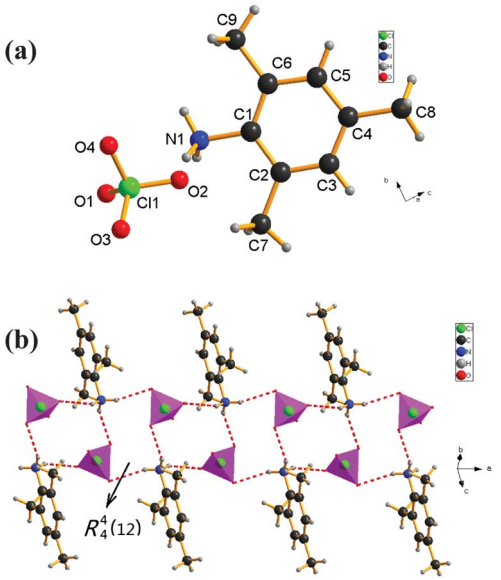

Fig. 2 (a) Compound **1** with the atomic numbering scheme at 25 °C. (b) Packing diagrams of **1** at 25 °C.

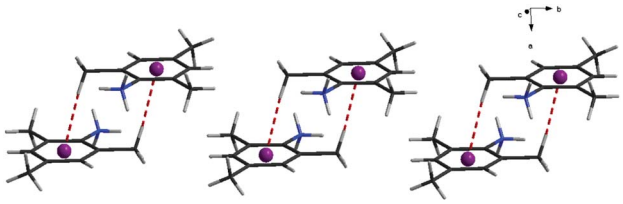

Fig. 3 The 2,4,6-trimethylanilinium ions stack head-to-tail with the C–H···π interactions at 25 °C.

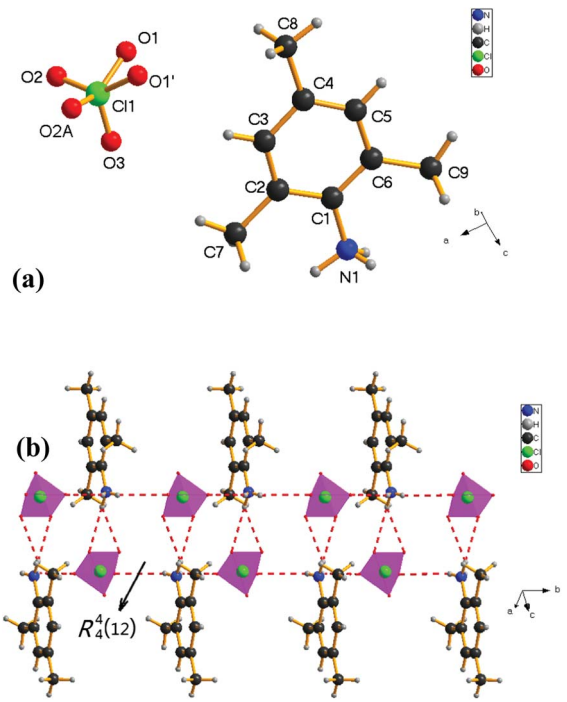

Fig. 4 (a) Compound **1** with the atomic numbering scheme at 110 °C (symmetry codes: x, 0.5 − y, z). (b) Packing diagrams of **1** at 110 °C.

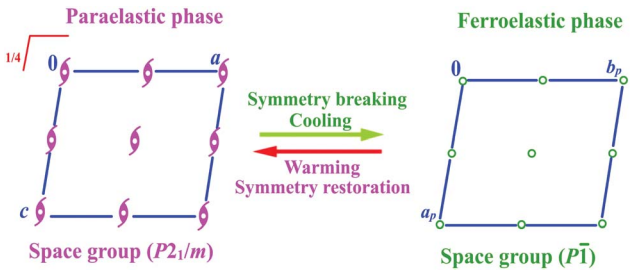

Fig. 5 Symmetry breaking process in **1** during temperature cooling down and warming up processes.

order to understand the structural changes of **1**, the room-temperature (25 °C) structure and the high-temperature (110 °C) structure have been measured, using the same crystal. The room temperature phase (RTP) structure is triclinic with a space group of $P\bar{1}$, and cell parameters of $a = 7.1581(14)$ Å, $b = 8.5937(17)$ Å, $c = 9.0642(18)$ Å, $\alpha = 88.74(3)°$, $\beta = 79.19(3)°$, $\gamma = 87.02(3)°$, $v = 546.90(19)$ Å^3. The high temperature phase (HTP) structure, carried out at 110 °C, is monoclinic and its space group turns to $P2_1/m$, with cell parameters of $a = 8.9084(18)$ Å, $b = 7.2253(18)$ Å, $c = 9.172(3)$ Å, $\alpha = 90°$, $\beta = 95.55°$, $\gamma = 90°$, $v = 587.6(3)$ Å^3. The unit cell parameters of **1** at the two different temperatures change abruptly and remarkably, indicating that **1** displays a reversible first-order phase transition, which matches well with the results of the DSC measurements.

3.2.1 Crystal of the RTP structure. The asymmetric unit of the RTP structure at 25 °C contains a protonated 2,4,6-trimethylanilinium cation, $(C_9H_{14}N)^+$, and an isolated tetrahedral perchlorate anion, ClO_4^- (Fig. 2a). The ClO_4^- anion shows typical Cl–O bond lengths [1.403(4)–1.422(4) Å] and the O–Cl–O angles range from 107.8(2)° to 111.0(3)°.

In compound **1**, $-NH_3^+$ groups of the 2,4,6-trimethylanilinium cation form three hydrogen bonds to oxygen atoms of the adjacent three ClO_4^- anions, respectively (Table 2S†). The Cl–O bond length for Cl atoms involved in hydrogen bonding is 1.403(4) and 1.419(4) Å. The N–H···O bonds between the 2,4,6-trimethylanilinium cations and perchlorate anions result in a noteworthy one-dimensional ribbon-like structure along the a-axis (Fig. 2b). This ribbon motif (Fig. 2b) is the dominant

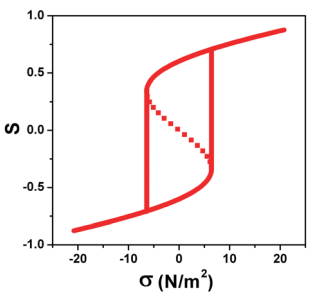

Scheme 1 The simulation strain–stress hysteresis loop in compound **1** showing that the relationship between strain and stress is nonlinear under Hooke's law ($S = \lambda\sigma$ where λ is the elastic constant).

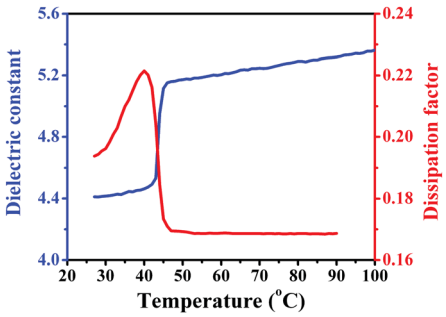

Fig. 6 Dielectric constants (ε') of compound **1** as a function of temperature (the measured frequency is fixed at 1 MHz).

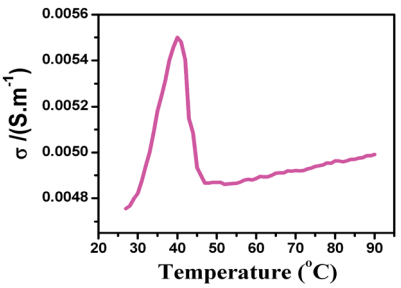

Fig. 7 Temperature dependence of the AC conductivity of compound **1** at the frequency of 1 MHz.

hydrogen-bonding motif in the structure of **1**, and the structure propagates *via* the $R^4_4(12)$ ring. The ammonium cations stack head-to-tail with the C–H···π interactions (Fig. 3).

3.2.2 Crystal of the HTP structure. The asymmetric unit of the HTP structure at 110 °C consists of one half 2,4,6-trimethylanilinium cation and one half perchlorate anion (Fig. 4a). In the ClO_4^- anion, the lengths of the Cl–O bond is 1.317(7) to 1.365(11) Å, which are shorter than those in RTP. In contrast to the RTP structure, the O1 atom of the perchlorate anion is disordered, which may result in the formation of higher symmetry. In compound **1**, the two components both lie on a common crystallographic mirror plane.

The N–H···O hydrogen bonds interaction are the main molecular interactions (Table 2S†). In **1**, the 2,4,6-trimethylanilinium cations and the ClO_4^- anions are stacked alternating along the *b*-axis, forming a ribbon-like structure parallel to the *b*-axis. The structure of **1** also propagates *via* the $R^4_4(12)$ ring. For the reason of the splitting of the O1 atom, the HTP structure has more hydrogen bonds than the RTP structure, resulting in the greater stability of the structure. The aromatic rings are parallel to the *ac*-plane and the adjacent aromatic rings are separated by a centroid-to-centroid distance of 5.59 Å, which is too long for π–π stacking interactions (Fig. 4b).

Symmetry breaking phenomenon occurs during the transition from the HTP to LTP, a total symmetry decreasing from four symmetric elements (E, C_2, i, σ_h) to two symmetric elements (E, i). Thus, this phase transition may be ferroelastic with an Aizu notion of $2/mF\bar{1}$.[15] Spatial symmetric operations change is shown in Fig. 5. Curie symmetry principle tells us that the space group at ferroeleastic phase should be the sub-space group at the paraelastic phase, *i.e.* its maximal non-isomorphic sub-groups containing Pm, $P2_1$ and $P\bar{1}$, respectively. Furthermore, spatial symmetric operation numbers decreases from 4 [(1) 1 (2) 2(0, 1/2, 0) 0, y, 0 (3) $\bar{1}$ 0, 0, 0 (4) m, x, 1/4, z] to 2 [(1) 1 (2) $\bar{1}$ 0, 0, 0] during symmetry breaking process in good agreement with macroscopic symmetry breaking.

Furthermore, we can use Landau theory to mimic the strain–stress hysteresis loop according to the equation of $\Delta G = \frac{1}{2}\alpha(T - T_c)S^2 + \frac{1}{4}\beta S^4 + \frac{1}{6}\gamma S^6 - S\sigma$, as shown in Scheme 1.

3.3 Dielectric properties

3.3.1 Dielectric constant and dielectric loss. As usual, phase transition is accompanied by an anomaly of the dielectric constant near the structural phase transition point. The phase transition of **1** is characterized by dielectric measurements. Because of the difficulty in obtaining large crystals, the powder-pressed pellet of **1** was used in the dielectric measurements. The real part of the dielectric constant of **1** was measured in the temperature range of 27 °C to 100 °C at 1 MHz (Fig. 6). In the temperature range of 27 °C to 42 °C, the dielectric constant almost remains unchanged (from *ca.* 4.41 to 4.47). Then it sharply increases to *ca.* 5.15 at about 46 °C, and then it is almost unchanged till 100 °C. The dielectric loss of **1** a1so displays an abrupt change (from *ca.* 0.22 to 0.16) at about 40 °C. The dielectric anomaly was observed during the measured temperature ranges, suggesting that there probably is a phase transition.

3.3.2 AC conductivity. The AC conductivity σ_{AC} was obtained from the imaginary part of the dielectric permittivity ε ($\varepsilon = \varepsilon' - i\varepsilon''$, where ε' and ε'' are the real and imaginary parts of the complex dielectric constant ε) by using the relation:

$$\sigma_{AC} = \omega\varepsilon''\varepsilon_0$$

where ω is the angular frequency $2\pi f$, and ε_0 the permittivity of free space ($\varepsilon_0 = 8.854 \times 10^{-12}$ F m^{-1}). Experimental values of the AC conductivity depends upon the frequency f. Fig. 7 shows the temperature dependence of the AC conductivity at the frequency 1 MHz. A drastic change of the conductivity of **1** occurred at about 40 °C. The observed behavior agreed with the results of the dielectric measurement.

4. Conclusion

In summary, we have discovered one organic–inorganic hybrid compound 2,4,6-trimethylanilinium perchlorate (**1**) undergoing first-order solid-state phase transitions at *ca.* 48 °C with abrupt changes in the cell parameters. The present work may open up a new avenue for the exploration of smart functional materials with phase transitions.

Acknowledgements

This work was supported by the National Natural Science Foundation of China (21101025, 20931002 and 90922005 as well as 21111140013), Jiangsu Planned Projects for Postdoctoral Research Funds (1101010B).

Notes and references

1 S. H. Baek, H. W. Jang, C. M. Folkman, Y. L. Li, B. Winchester, J. X. Zhang, Q. He, Y. H. Chu, C. T. Nelson, M. S. Rzchowski, X. Q. Pan, R. Ramesh, L. Q. Chen and C. B. Eom, *Nat. Mater.*, 2010, **9**, 309.

2 V. Nagarajan, A. Roytburd, A. Stanishevsky, S. Prasertchoung, T. Zhao, L. Chen, J. Melngailis, O. Auciello and R. Ramesh, *Nat. Mater.*, 2002, **2**, 43.

3 M. C. Gallardo, J. Manchado, F. J. Romero, J. Cerro, E. K. H. Salje, A. Planes, E. Vives, R. Romero and M. Stipcich, *Phys. Rev. B*, 2010, **81**, 174102.

4 M. D. Hollingsworth, M. L. Peterson, J. R. Rush, M. E. Brown, M. J. Abel, A. A. Black, M. Dudley, B. Raghothamachar, U. Werner-Zwanziger, E. J. Still and J. A. Vanecko, *Cryst. Growth Des.*, 2005, **5**(6), 2100.

5 Y. Yamada, *Phys. Rev. B*, 1992, **46**, 5906.

6 N. A. Spaldin and M. Fiebig, *Science*, 2005, **309**, 391.

7 W. Eerenstein, N. D. Mathur and J. F. Scott, *Nature*, 2006, **442**, 759.

8 T. Kimura, T. Goto, H. Shintani, K. Ishizaka, T. Arima and Y. Tokura, *Nature*, 2003, **426**, 55.

9 N. Hur, S. Park, P. A. Sharma, J. S. Ahn, S. Guha and S. W. Cheong, *Nature*, 2004, **429**, 392.

10 (*a*) D.-W. Fu, Y.-M. Song, G.-X. Wang, Q. Ye, R.-G. Xiong, T. Akutagawa, T. Nakamura, P. W. H. Chan and S. D. Huang, *J. Am. Chem. Soc.*, 2007, **129**, 5346; (*b*) W. Zhang, R.-G. Xiong and S. D. Huang, *J. Am. Chem. Soc.*, 2008, **130**, 10468; (*c*) H.-Y. Ye, D.-W. Fu, Y. Zhang, W. Zhang, R.-G. Xiong and S. D. Huang, *J. Am. Chem. Soc.*, 2009, **131**, 42; (*d*) W. Zhang, L.-Z. Chen, R.-G. Xiong, T. Nakamura and S. D. Huang, *J. Am. Chem. Soc.*, 2009, **131**, 12544; (*e*) W. Zhang, H.-Y. Ye, H.-L. Cai, J.-Z. Ge, R.-G. Xiong and S. P. D. Huang, *J. Am. Chem. Soc.*, 2010, **132**, 7300; (*f*) T. Hang, W. Zhang, H.-Y. Ye and R.-G. Xiong, *Chem. Soc. Rev.*, 2011, **40**, 3577; (*g*) H.-L. Cai, W. Zhang, J.-Z. Ge, Y. Zhang, K. Awaga, T. Nakamura and R.-G. Xiong, *Phys. Rev. Lett.*, 2011, **107**, 147601; (*h*) D.-W. Fu, W. Zhang, H.-L. Cai, Y. Zhang, R.-G. Xiong, S. D. Huang and T. Nakamura, *Angew. Chem., Int. Ed.*, 2011, **50**, 11947; (*i*) D.-W. Fu, W. Zhang, H.-L. Cai, Y. Zhang, J. Z. Ge, R.-G. Xiong and S. D. Huang, *J. Am. Chem.Soc.*, 2011, **133**, 12780; (*j*) D.-W. Fu, W. Zhang, H.-L. Cai, J.-Z. Ge, Y. Zhang and R.-G. Xiong, *Adv. Mater.*, 2011, **23**, 5658; (*k*) G.-C. Xu, W. Zhang, X.-M. Ma, Y.-H. Chen, L. Zhang, H.-L. Cai, Z.-M. Wang, R.-G. Xiong and S. Gao, *J. Am. Chem. Soc.*, 2011, **133**, 14948; (*l*) W. Zhang and R.-G. Xiong, *Chem. Rev.*, 2012, **112**, 1163.

11 V. K. Wadhawan, *Bull. Mater. Sci.*, 1984, **6**, 733.

12 E. K. H. Salje, *Contemp. Phys.*, 2000, **41**, 79.

13 H. Schmid, *J. Phys.: Condens. Matter*, 2008, **20**, 4201.

14 M. P. Cruz, Y. H. Chu, J. X. Zhang, P. L. Yang, F. Zavaliche, Q. He, P. Shafer, L. Q. Chen and R. Ramesh, *Phys. Rev. Lett.*, 2007, **99**, 7601.

15 K. Aizu, *Phys. Rev. B*, 1970, **2**, 754.